Journal of Alloys and Compounds 480 (2009) 541–546

Contents lists available at ScienceDirect

Journal of Alloys and Compounds

journal homepage: www.elsevier.com/locate/jallcom

Investigations of GaN metal-oxide-semiconductor capacitors with sputtered HfO_2 gate dielectrics

C.F. Shih[a,b,*], K.T. Hung[a], C.Y. Hsiao[a], S.C. Shu[a], W.M. Li[a]

[a] Department of Electrical Engineering, National Cheng Kung University, Tainan 70101, Taiwan
[b] Center for Micro/Nano Science and Technology, National Cheng Kung University, Tainan 70101, Taiwan

ARTICLE INFO

Article history:
Received 12 December 2008
Received in revised form 14 January 2009
Accepted 22 January 2009
Available online 14 February 2009

Keywords:
GaN
MOS
HfO_2
Sputter

ABSTRACT

This work elucidates the properties of Al/HfO_2/GaN metal-oxide-semiconductor capacitors using reactively sputtered HfO_2 as a gate dielectric. The influence of GaN surface treatments and the post-annealing of HfO_2 films on the leakage current, flat-band voltage, interface trap densities, dielectric constants, and effective oxide charges of the GaN MOS capacitors are presented. The Ga oxynitride on the surface of GaN was effectively removed by chemical solutions that also slightly reduced the dielectric constant, slightly increased the flat-band voltage, eliminated the hysteresis of the capacitance–voltage measurement, and yielded a similar leakage to that without surface treatment. A highest dielectric constant of HfO_2 (17) was obtained when the sample was annealed at 600 °C for 20 min, while the lowest interface trap density (5.3×10^{11} cm^{-2}) was obtained when the sample was annealed at 800 °C for 40 min. The leakage mechanism was well fitted by the Schottky emission and Frenkel–Poole emission models at a lower and higher electric field.

III-Nitride semiconductors have been demonstrated to have potential applications in high-power, high-speed, and high-temperature devices because of their attractive fundamental properties such as high direct band-gap, chemical stability and high electron saturation velocity. Recently, GaN-based transistors such as metal-semiconductor field-effect-transistors (MES-FETs), hetero-junction FETs (HFETs), and high-electron-mobility transistors (HEMTs) have been reported [1–4]. All such devices suffer from the gate leakage problem. A large leakage current flows at the metal and GaN interface, making a good Schottky contact difficult to achieve. Metal-oxide-semiconductor FETs (MOS-FETs) and MOS-HFETs with an oxide interlayer between the metal and the semiconductor have much smaller leakage currents. Therefore, GaN-based MOS-FETs and MOS-HFETs have been important topics of research [5–8].

GaN-based MOS-FETs provide a number of advantages over Si-based devices. MOS capacitors are good forerunners of MOS-FETs or MOS-HFETs that can be employed to study the properties of the semiconductor–insulator interface. Previously, numerous gate dielectrics, such as Ga_2O_3, SiO_2, Si_3N_4, Al_2O_3, HfO_2, MgO, SiN_xO_y, Ta_2O_5, and ZrO_2 [9–16] have been studied using MOS structures. Among these, HfO_2 has attracted the most attention by far due to its good thermal stability and high dielectric constant. Optimizing the GaN MOS structure involves two major challenges—lowering the interface traps and improving the oxide quality. Many effective techniques are available for depositing insulators on GaN. They include plasma-enhanced chemical vapor deposition (PE-CVD), e-beam evaporation, low-pressure CVD, photo-CVD, sputtering and atomic layer deposition [10–12,14,15]. Among these techniques, sputtering offers the advantages of simplicity process, low cost and high throughput. Besides, various chemical solutions such as H_3PO_4, $H_2SO_4 + H_2O_2$, H_3PO_4, HF, and HCl have been applied to clean the GaN surface prior to the oxide deposition [9–13]. The performance of the MOS capacitors depends sensitively on the surface chemistry of as-grown GaN. However, the relationship between surface treatments of GaN and corresponding MOS properties has not been elucidated. Moreover, no research into GaN MOS capacitors with a sputtered HfO_2 as an oxide layer has been conducted.

This work systematically studies the Al/HfO_2/GaN MOS capacitor using reactively sputtered HfO_2 as an insulator. The effect of GaN surface treatments and the annealing conditions of HfO_2 films on the leakage current, flat-band voltage, interface traps densities, dielectric constants and effective oxide charges of the GaN MOS capacitors are presented. The dominant leakage mechanism is also described.

1. Experimental

N-type GaN films were grown on (0 0 0 1) sapphire substrate by metal-organic chemical vapor deposition (Aixtron rf-200/4). A low-temperature GaN nucleation

* Corresponding author at: Department of Electrical Engineering, National Cheng Kung University, Tainan 70101, Taiwan. Tel.: +886 6 2757575x62398; fax: +886 6 2080687.
E-mail address: cfshih@mail.ncku.edu.tw (C.F. Shih).

0925-8388/$ – see front matter © 2009 Elsevier B.V. All rights reserved.
doi:10.1016/j.jallcom.2009.01.141

layer, 25 nm thick, was first deposited at 520 °C. This was followed by a 1.5 μm GaN grown at 1050 °C. Although the threading dislocations of GaN could be reduced by increasing the thickness, the thickness of GaN was well chosen to yield a favorable surface flatness, which is key to a metal–semiconductor interface, with help of the *in situ* reflectmetry using an 500 nm monochromatic light. The precursors were trimethylgallium (TMG) for Ga, ammonia for nitrogen and silane for n-type doping, with hydrogen carrier gas. The Si doping concentration was around 2×10^{18} cm^{-3}. Before the oxide layers were deposited, the GaN samples were prepared by sequentially rinsing in de-ionized (DI) water, hot acetone, IPA, DI water, chemical solution (5 min), and finally repeating DI water/hot acetone/IPA/DI water rinsing. The chemical solutions adopted herein included diluted hydrochloric acid (HCl, H_2O:HCl = 1:1), buffer oxide etchant (H_2O:HF = 50:1) and potassium hydroxide (KOH, 1 M). HfO_2 thin films were deposited by reactive sputtering (dc, 200 W) using Hf metal as a target, in an Ar/O_2 ambient (Ar:O_2 = 10:5 sccm). The background and working pressure during sputtering were 1×10^{-6} and 5×10^{-3} Torr, respectively. The as-deposited HfO_2 was thermally annealed at temperatures from 500 to 800 °C, for 5, 20, 40, and 60 min. The circular 250 nm-thick Al gate electrode was formed by e-beam evaporation. The optimized post-annealing condition of the metal electrodes (10 min in nitrogen ambient at 400 °C) was used throughout. Binding energies was obtained by high-resolution X-ray photoemission spectroscopy (HRXPS, Ulvac/PHI Quantera SXM). The grazing-incident X-ray diffraction (GIXRD, Rigaku D/MAX2500) was used to characterize the phase of HfO_2 films. The electrical properties of the fabricated MOS capacitors were characterized by measuring high-frequency capacitance–voltage (*C–V*) and current density–voltage (*J–V*) curves with an Agilent 4294A precision impedance analyzer and an Agilent semiconductor parameter analyzer (E5270B mainframe with module E5287A), respectively.

2. Results and discussion

Quantitative analysis of the as-grown HfO_2 thin films by HR-XPS indicated that the compositional ratio of O/Hf approached 2 (not shown), even without thermal annealing, indicating a good stoichiometry manipulation of the sputtering. HR-XPS was also conducted to examine the HfO_2/GaN interface. The GaN surfaces of the samples studied herein were treated with different aqueous solutions but all the HfO_2 thin films were deposited under identical conditions. *In situ* Ar^+ ion sputtering was used to remove slowly the HfO_2 until the underlying Ga 2p signals appeared during HR-XPS measurement. Fig. 1(a) and (b) plots corresponding data for O 1s and Ga 2p, respectively. The bottom profile is constructed from signals from the as-grown GaN for comparison. Both the O 1s and Ga 2p signals were shifted to a binding energy that was approximately 2 eV lower than that of untreated GaN. These shifts were independent of the chemical solutions selected. All of the broad Ga $2p_{1/2}$ peaks in the vicinity of 1115 eV for the chemical treated samples could be deconvoluted into two peaks, exhibiting a chemical shift of ~2 eV, indicating a Ga oxynitride interfacial layer was presented. The origin of the interlayer is ascribed to the initial stages of sputtering because no such signal form the as-cleaned GaN surfaces could be resolved.

The effects of surface treatments on the electrical properties of GaN MOS diodes were studied by comparing the KOH, HCl, and BOE treated samples. An untreated sample was used for reference. The leakage currents for all of the treated and non-treated MOS samples were as small as $\sim 2 \times 10^{-9}$ A/cm^2 (Fig. 2(a)). Surface treatments

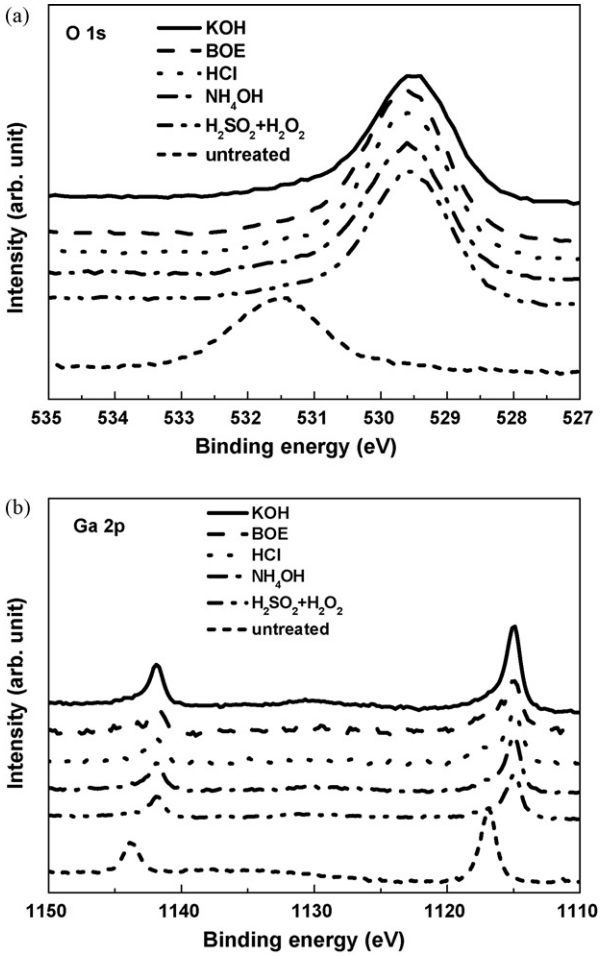

Fig. 1. HR-XPS profiles of the GaN/HfO_2 interfaces: (a) O 1s and (b) Ga 2p.

caused small deviations of the leakages. Regardless of treatment methods, the leakage current of MOS capacitor declined as the HfO_2 thickness increased (Fig. 2(b)), indicating that the main leakage current comes from the oxide layers not the interfaces. Fig. 2(c) plots well-behaved *C–V* curves that were measured at 1 MHz. No frequency dispersion was observed (100 kHz to 1 MHz), suggesting that the films have promising dielectric properties. Electrical hysteresis of the *C–V* curves due to the trapped charges within the oxide layers of the non-treated samples was observed, but decreased to a negligible level upon treatment with aqueous solution. Since the HfO_2 films were deposited under the same conditions, the hysteresis behavior was attributed to the native Ga oxynitride over the as-grown GaN surface. Moreover, the surface-treated samples had a lower accumulation capacitance than the non-treated one. From

Table 1
ε_{GaN}, *EOT*, V_{FB}, N_{eff} and D_{it} values for Al/HfO_2/GaN MOS capacitors with different annealing temperatures and times.

Temperature (°C)	Time (min)	ε_{GaN}	*EOT* (nm)	V_{FB} (V)	N_{eff} ($\times 10^{12}$ cm^{-2})	D_{it} ($\times 10^{11}$ cm^{-2})
600	20	17	8.1	0.77	2.1	8.1
	40	14	10.1	0.75	1.6	6.8
	60	14	9.9	0.67	1.5	6.6
700	20	13		0.85	1.7	10.4
	40	11	12.6	0.86	1.4	9.5
	60	10	13.8	0.79	1.3	7.4
800	20	14	10.2	0.73	2.0	6.4
	40	12	11.2	0.72	1.5	5.3

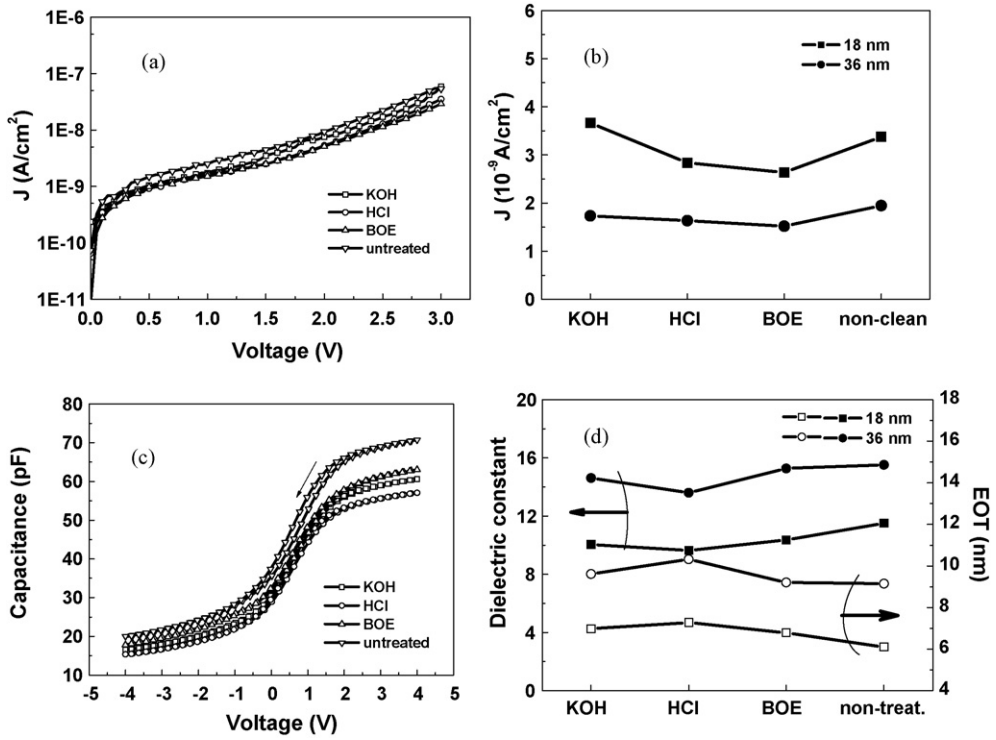

Fig. 2. Electrical properties of the Al/HfO_2/GaN MOS capacitors with different surface treatments of GaN and HfO_2 thickness. (a) *J–V* curves, (b) leakage currents at a +1 V gate bias, (c) high-frequency *C–V* curves and (d) dielectric constants and *EOT* values of HfO_2. The *C–V* curves were measured from two sweep directions. The electrical hysteresis was presented for the non-treated sample.

the accumulation capacitance (C_{ox}), the dielectric constants (ε_{ox}) are derived using:

$$C_{ox} = \frac{\varepsilon_{ox}\varepsilon_0 A}{t_{ox}}, \quad (1)$$

where ε_0 is the permittivity of a vacuum; t_{ox} = 18 nm (or 36 nm) is the oxide thickness, determined by transmission electron microscopy (not shown), and $A = 2 \times 10^{-4}$ cm^{-2} is the area of the capacitors. The equivalent oxide thickness (*EOT*), without deducting the quantum mechanical effect is defined as

$$EOT = \frac{\varepsilon_{SiO_2}}{\varepsilon_{ox}} t_{ox}, \quad (2)$$

where $\varepsilon_{SiO_2} = 3.9$ is the dielectric constant of SiO_2. Fig. 2(d) plots the calculated dielectric constants of HfO_2 and *EOT* for the various surface treatment methods. The similarity among the degrees of leakage reveals that these samples had similar dielectric constants and *EOT*. Notably, thicker oxides are associated with larger dielectric constants (Fig. 2(d)), perhaps because of the improvement of the crystallinity. The capacitance of the n-GaN surface under the flat-band condition is expressed as

$$C_{FBS} = \frac{\varepsilon_{GaN}\varepsilon_0}{\lambda_n}, \quad (3)$$

where $\lambda_n = (\varepsilon_{GaN}\varepsilon_0 kT/e^2 N_D)^{1/2}$ is the extrinsic Debye length; ε_{GaN} = 8.9 is the dielectric constant of GaN; k is the Boltzmann constant; T is the absolute temperature; e is the electronic charge, and $N_D = 2 \times 10^{18}$ cm^{-3} is the doping concentration. If the surface states of GaN are ignored, the flat-band capacitance, C_{FB}, can be calculated by substituting C_{FBS} from Eq. (3) into the series capacitance relationship:

$$\frac{1}{C_{FB}} = \frac{1}{C_{ox}} + \frac{1}{C_{FBS}}. \quad (4)$$

Thus, the flat-band voltage (V_{FB}) is obtained from the high-frequency *C–V* curves (Fig. 2(c)), plotted in Fig. 3(a). The difference between the metal-semiconductor work functions (ϕ_{Ms}) for Al metal and n-GaN is about −0.05 eV by calculation, indicating that the MOS diodes can be under flat-band condition at near zero gate bias. The deviation of ϕ_{Ms} and V_{FB} yields the effective oxide charges, $Q_{eff} = Q_{ot} + Q_m + Q_f$, using

$$Q_{eff} = \frac{C_{ox}(\phi_{ms} - V_{FB})}{A}, \quad (5)$$

where Q_{ot} denotes the oxide trapped charge density; Q_m is the mobile ionic charge density, and Q_f is the fixed charge density. Dividing the Q_{eff} by $e = 1.6 \times 10^{-19} C$ yields the effective number density (N_{eff}) of the oxides. From the normalized C_{FB}/C versus V curves yield the interface state density (D_{it}) was calculated according to the well-known Terman method for MOS structures [17]. Fig. 3(a)–(c) plots the results of comparative studies of V_{FB}, N_{eff} and D_{it} of the MOS samples, with and without GaN surface treatments. Fig. 3(a) reveals that the V_{FB} shifted positively as HfO_2 thickness increased. The dependence of V_{FB} on thickness revealed that the fixed charges were uniformly located throughout the bulk HfO_2. Since the shift of V_{FB} came mostly from the oxide charges, the V_{FB} values of various treated samples were similar. The calculated N_{eff} in Fig. 3(b) confirmed this phenomenon. Fig. 3(c) indicates that the density of the interface charges of non-treated sample was lower than that of the chemically treated samples. We suggest two explanations. (1) The oxides on the GaN surface were removed using chemical solutions that also damaged the GaN surface. Thus, the surface defects contributed to the D_{it} of the GaN/HfO_2 interfaces. However, this possibility was ruled out because HR-XPS revealed no obvious chemical shift of the as-treated GaN surface. (2) A thin interfacial layer formed in the initial deposition of HfO_2. According to Fig. 2(c) and based on the series capacitance, this interfacial layer may have a lower dielectric constant but fewer oxide traps than the

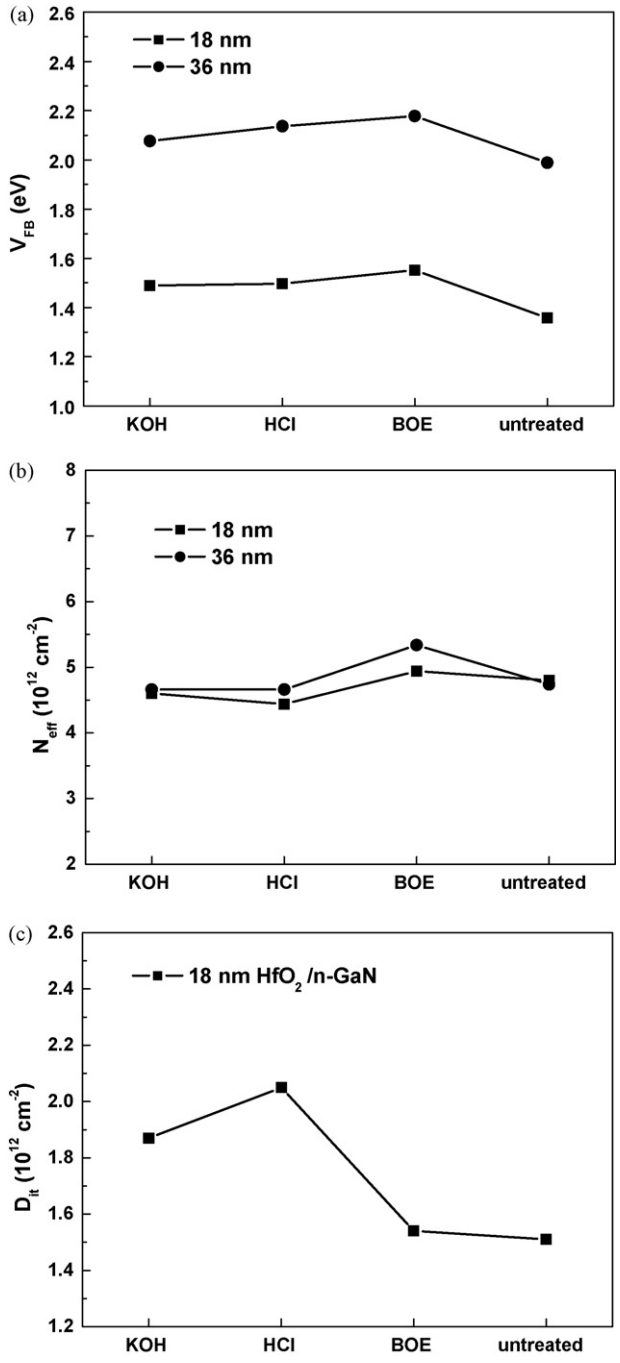

Fig. 3. (a) Flat-band voltage (V_{FB}), (b) effective numbers density of oxide (N_{eff}) and (c) interface trap densities for the GaN MOS capacitors with various surface treatments. The thickness of HfO_2 films were 18 and 36 nm.

native Ga oxynitride layer. Moreover, the Ga oxynitride layer of the as-grown GaN may act as a barrier to the radiation damage. The latter reason suggests that a buffer layer between the sputtered HfO_2 and the chemically treated n-GaN may be essential to further improvement.

Fig. 4 displays the GIXRD patterns of the 18 nm-thick-HfO_2 thin films annealed at elevated temperatures for 30 min. Monoclinic-related peaks became stronger and sharper as the temperature increased. An obvious transition from amorphous-like to monoclinic occurred when the annealing temperature exceeded 600 °C. Fig. 5 plots the leakage current density in the MOS capacitors that

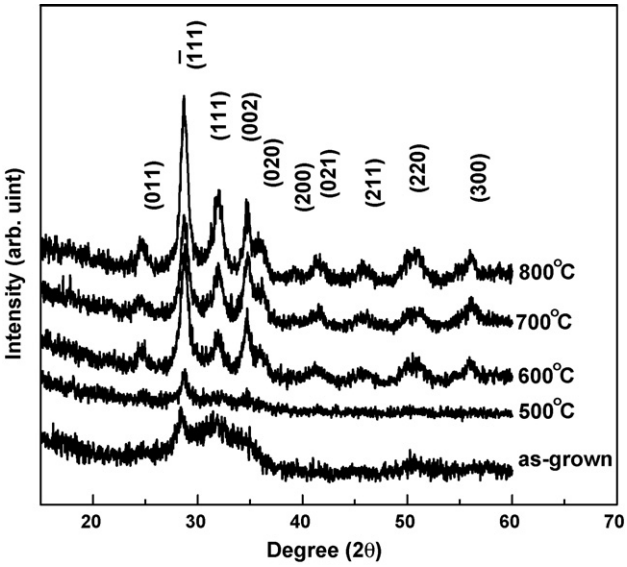

Fig. 4. GIXRD patterns for the HfO_2 annealed at temperatures from 500 to 800 °C.

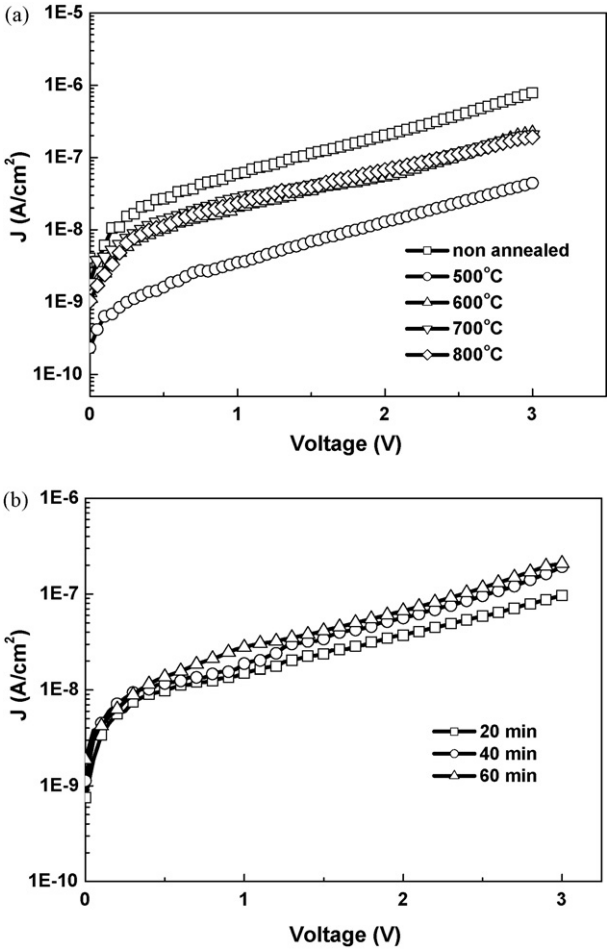

Fig. 5. *J–V* curves of GaN MOS capacitors with HfO_2 annealed (a) at 500–800 °C for 40 min and (b) at 700 °C for 20–60 min. All of the samples were annealed in N_2 ambient.

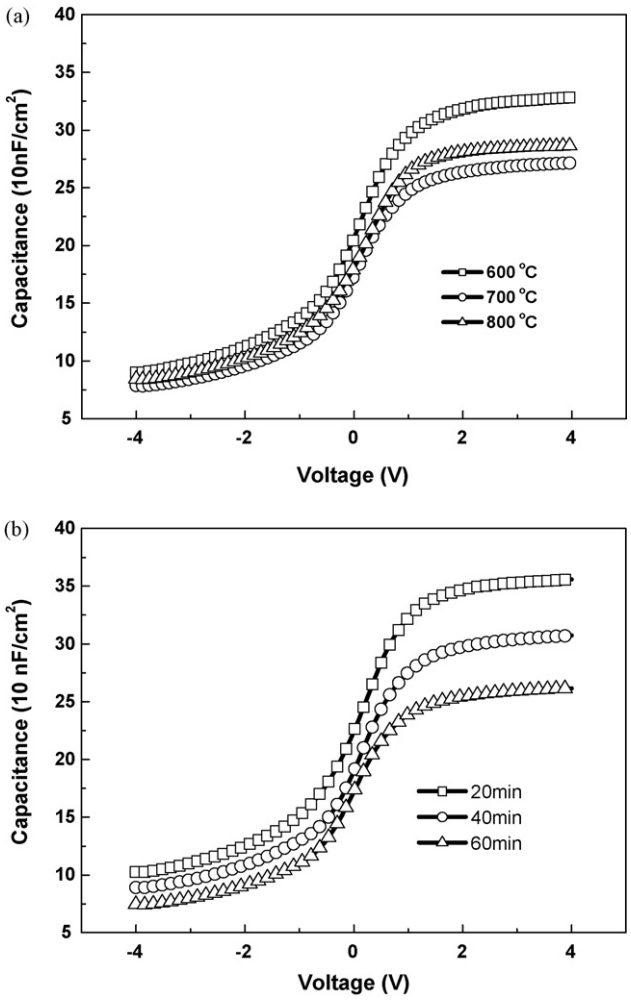

Fig. 6. *C–V* curves of the GaN MOS capacitors with HfO_2 annealed (a) at 500–800 °C for 40 min and (b) at 700 °C for 20–60 min. All of the samples were annealed in N_2 ambient.

were annealed at various temperatures as a function of time. The leakage current density at a +1 V gate bias was markedly reduced from 7×10^{-8} to 3×10^{-9} A/cm^2 upon annealing at 500 °C (Fig. 5(a)). The leakage current density increased to about 2×10^{-8} A/cm^2 as the annealing temperatures increased (600–800 °C), because of grain boundaries were formed by high-temperature annealing. Changes in the annealing time at 700 °C in N_2 ambient had little effect on the leakage behaviors (Fig. 5(b)). Fig. 6(a) and (b) presents the *C–V* profiles of the MOS with different post-annealing temperatures and times. The oxide capacitance decreased as the annealing time increased. The highest dielectric constant, lowest N_{eff}, and lowest D_{it} within the experiment were found to be 17 (600 °C, 20 min), 1.3×10^{12} cm^{-2} (700 °C, 60 min) and 5.3×10^{11} (800 °C, 40 min), respectively. Table 1 presents more ε_{GaN}, *EOT*, V_{FB}, N_{eff} and D_{it} values of the Al/HfO_2/GaN MOS capacitors with different annealing temperatures and times. These values decreased as the annealing time increased.

The *J–V* characterization of MOS capacitor with moderate electrical properties (HfO_2 annealed at 700 °C, 40 min) was studied to understand further the leakage behaviors. The Schottky emission mechanism [18] is described by

$$J = A * T^2 \exp\left[\frac{-e(\phi_B - \sqrt{eE/4\pi\varepsilon_r\varepsilon_0})}{kT}\right], \quad (6)$$

where the effective Richardson constant A^* is a function of electron effective mass in oxide; J is the current density; k is the Boltzmann constant; h is the Planck constant; E is the electric field; ε_r is the dynamic dielectric constant, and ϕ_B is the Schottky barrier height. This equation was used to fit the leakage current behaviors in the low electric field side (0.3–0.75 MV/cm) of the ln$J$ versus $\sqrt{E}$ plot. The leakage current in an electric field in the range of 0.3–0.75 MV/cm was fitted well with the Schottky emission mechanism (Fig. 7(a)). The ln$J$ versus $\sqrt{E}$ plot also yields ϕ_B and ε_r as 1.12 eV and 9.3, respectively. The ε_r calculated from this model was close to, but a little lower than the high-frequency *C–V* measurement. Notably, the value of ϕ_B was very close to the conduction band offset (~1.1 eV) at the GaN/HfO_2 interface that was calculated using methods based on the charge neutrality [19]. When the electric field exceeded 0.75 MV/cm, the ln$J$–$\sqrt{E}$ plot positively diverged from the Schottky emission mode, indicating that additional leakage paths contributed to the leakage current. The ln(J/E) versus $\sqrt{E}$ curve, plotted in Fig. 7(b), are fitted well by the Frenkel–Poole (FP) emission model, which is given by [20]

$$J \propto E \exp\left[\frac{-q(\phi_B - \sqrt{eE/4\pi\varepsilon_r\varepsilon_0})}{kT}\right]. \quad (7)$$

The leakage characteristics indicate that the electron emission from the defect states within the oxide layer started when the electric field exceeded their activation energies.

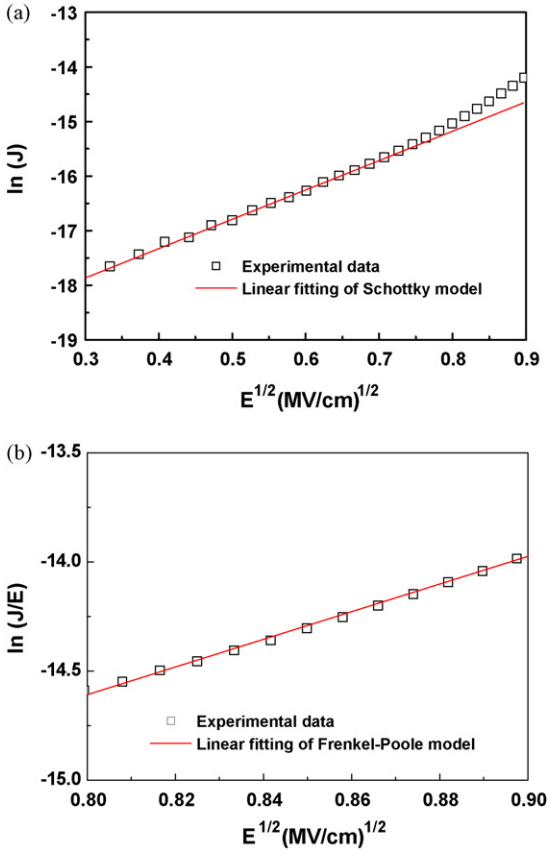

Fig. 7. (a) Schottky and (b) Frenkel–Poole emission models fitted for the leakage behaviors of GaN MOS capacitors.

3. Conclusion

HfO_2 films were deposited on the n-type GaN by a reactive sputtering. The Al/HfO_2/GaN MOS capacitors using the sputtered HfO_2 gate dielectric were investigated. The influence of GaN surface treatments and the post-annealing of HfO_2 films on the leakage current, flat-band voltage, interface trap densities, dielectric constants, and effective oxide charges of the GaN MOS capacitors were presented. The Ga oxynitride on the surface of GaN was effectively removed by chemical solutions that also slightly reduced the dielectric constant, slightly increased the flat-band voltage, eliminated the hysteresis of the capacitance–voltage measurement, and yielded a similar leakage to that without surface treatment. BOE treated sample showed lowest interface trap density to the other methods. A highest dielectric constant of HfO_2 (17) was obtained when the sample was annealed at 600 °C for 20 min, while the lowest interface trap density (5.3×10^{11} cm^{-2}) was obtained when the sample was annealed at 800 °C for 40 min. The ε_{GaN}, *EOT*, V_{FB}, N_{eff}, and D_{it} decreased monotonically as the annealing time increased. The leakage mechanism was well fitted by the Schottky emission and Frenkel–Poole emission model at a lower and higher electric field.

Acknowledgements

This work was supported by the National Science Council under contract no. NSC-96-2221-E-006-288-MY2 and Center for Micro/Nano Science and Technology.

References

[1] A. Koudymov, G. Simin, M.A. Khan, A. Taraki, R. Gaska, M.S. Shur, IEEE Electron Device Lett. 24 (2003) 680.
[2] C.Q. Chen, J.P. Zhang, V. Adivarahan, A. Koudymov, J. Fatima, G. Simin, J. Yang, M.A. Khan, Appl. Phys. Lett. 82 (2003) 4593.
[3] Y.K. Su, S.C. Wei, R.L. Wang, S.J. Chang, C.H. Ko, T.M. Kuan, IEEE Electron Device Lett. 24 (2003) 622.
[4] Y. Irokawa, B. Luo, F. Ren, C.C. Pan, G.T. Chen, J.I. Chyi, S.S. Park, Y.J. Park, S.J. Pearton, Electrochem. Solid-State Lett. 7 (2004) G8.
[5] M. Asif Khan, X. Hu, A. Tarakji, G. Simin, J. Yang, R. Gaska, Ms.S. Shur, Appl. Phys. Lett. 77 (2000) 1339.
[6] W. Huang, T. Khan, T.P. Chow, IEEE Electron Device Lett. 27 (2006) 796.
[7] K. Matocha, T. Paul Chow, R.J. Gutmann, IEEE Trans. Electron Device 52 (2005).
[8] P.D. Ye, B. Yang, K.K. Ng, J. Bude, G.D. Wilk, S. Halder, J.C.M. Hwang, Appl. Phys. Lett. 86 (2005) 063501.
[9] C.T. Lee, H.W. Chen, H.Y. Lee, Appl. Phys. Lett. (2003) 4304.
[10] K. Matocha, R.J. Gitmann, T. Paul Chow, IEEE Trans. Electron Device 50 (2005) 1200.
[11] S. Arulkumaran, T. Egawa, H. Ishikawa, T. Jimbo, M. Umeno, Appl. Phys. Lett. 73 (2003) 809.
[12] Y.C. Chang, H.C. Chiu, Y.J. Lee, M.L. Huang, K.Y. Lee, M. Hong, Y.N. Chiu, J. Kwo, Y.H. Wang, Appl. Phys. Lett. 90 (2007) 232904.
[13] J. Kim, B. Gila, R. Mahandru, J.W. Johnson, J.H. Shin, K.P. Lee, B. Luo, A. Onstine, C.R. Abernathy, S.J. Pearton, Ren, J. Electrochem. Soc. 149 (2002) G482.
[14] S.J. Chang, C.K. Wang, Y.K. Su, C.S. Chang, T.K. Lin, T.K. Ko, H.L. Liu, J. Electrochem. Soc. 152 (2005) G423.
[15] L.W. Tu, W.C. Kuo, K.H. Lee, P.H. Tsao, C.M. Lai, A.K. Chu, J.K. Sheu, Appl. Phys. Lett. 77 (2000) 3788.
[16] S. Abermann, G. Pozzovivo, J. Kuzmik, G. Strasser, D. Pogany, J.-F. Carlin, N. Grandjean, E. Bertagnolli, Semicond. Sci. Technol. 22 (2007) 1272.
[17] L.M. Terman, Solid-State Electron. 5 (1962) 258.
[18] T. Yamaguchi, H. Satake, N. Fukushima, A. Toriumi, Tech. Dig.: Int. Electron Devices Meet (2000) 19.
[19] J. Robertson, B. Falabretti, J. Appl. Phys. 100 (2005) 014111.
[20] J. Frenkel, Phys. Rev. 54 (1938) 647.